J. Coat. Technol. Res., **15** (5) 899–911, 2018
https://doi.org/10.1007/s11998-017-0039-y

Slot die stripe coating of low viscous fluids

Sebastian M. Raupp, Marcel Schmitt, Anna-Lena Walz, Ralf Diehm, Helga Hummel, Philip Scharfer, Wilhelm Schabel

Abstract Slot die coating is applied to deposit thin and homogenous films in roll-to-roll and sheet-to-sheet applications. The critical step in operation is to choose suitable process parameters within the process window. In this work, we investigate an upper limit for stripe coatings. This maximum film thickness is characterized by stripe merging which needs to be avoided in a stable process. It is shown that the upper limit reduces the process window for stripe coatings to a major extent. As a result, stripe coatings at large coating gaps and low viscosities are only possible for relatively thick films. Explaining the upper limit, a theory of balancing the side pressure in the gap region in the cross-web direction has been developed.

Keywords Slot die coating, Stripe coating, Process window, Minimum film thickness, Upper limit, Low viscous liquids, Model for film spreading

Electronic supplementary material The online version of this article (https://doi.org/10.1007/s11998-017-0039-y) contains supplementary material, which is available to authorized users.

S. M. Raupp (✉), M. Schmitt, A.-L. Walz, R. Diehm, P. Scharfer, W. Schabel
Institute of Thermal Process Engineering, Thin Film Technology, Karlsruhe Institute of Technology, Karlsruhe, Germany
e-mail: sebastian.raupp@kit.edu

S. M. Raupp, R. Diehm, P. Scharfer
InnovationLab, Heidelberg, Germany

H. Hummel
Chemistry and Biotechnology, University of Applied Sciences, FH Aachen, Jülich, Germany

Letters

CF	Correction factor
ETOH	Ethanol
h	Height (z-axis) (μm)
l	Length (x-axis) (mm)
n	Power law exponent
p	Pressure (mbar)
PAA	Polyacrylamide
q	Specific volume flow (m^2/min)
t	Time (s)
u	Speed (m/min)
w	Width (y-axis) (mm)
x	x-axis in web direction
y	y-axis in cross-web direction

Greek letters

$\dot{\gamma}$	Shear rate (1/s)
η	Newtonian viscosity (Pa s)
θ	Static contact angle (°)
ϑ	Dynamic contact angle (°)
κ	Consistency factor (Pa s^e)
σ	Surface tension (mN/m)

Indices

approx.	Approximated
Bead	Bead
Ca	Capillary number
Cap	Capillary
crit	Critical
D	Downstream
G	Gap
Fluid	Fluid

max	Maximum
min	Minimum
s	Slot
Side	Side
solid	Solid
spacer	Spacer
spread	Spread
U	Upstream
Vac	Vacuum
w	Web
wet	Wet
1	Position 1
2	Position 2
3	Position 3

Introduction

In the field of organic electronics, the precise control of coating thickness and coating width is crucial.[1] The slot die coating method is applicable to precisely deposit a wide range of wet film thicknesses from the range of one micron[2] to hundreds of microns.[1,3–5]

However, coating defects might occur[6–8] if the process parameters are not chosen appropriately within a specific process window. To obtain defect-free coatings, the coating bead between die and substrate needs to be stable during the operation. Stable conditions are achieved if the bead of menisci are fully established and pinned stationary. Two major mechanisms limiting the menisci are known from the literature. First, the so-called low-flow limit[9] restricts the stability of the meniscus at the downstream lip.[10,11] Upon failure, the downstream meniscus cannot withstand the local pressure difference and air penetrates from the downstream side. This results in web-direction lines called ribbing and uncoated streaks.[8] Second, the dynamic wetting failure described by the visco-capillary model restricts the stability at the upstream, e.g., against upstream air entrainment.[4,6,12]

Regarding the width of the coated film and the geometry of its edges, the menisci rectangular to the coating direction are most important. Depending on fluid acceleration, surface tension, and viscosity as well as die geometry, neck-in[4,8,13] can appear. A neck-in leads to super elevations at the edges of the film which can be a problem, especially, for multilayer-stacked devices. Coating velocities range from less than 1 m/min[14–19] in sheet-to-sheet to more than 100 m/min[20,21] in roll-to-roll applications.

Slot die coating is mainly applied for full-area coatings. Beyond that, structured coatings[1,22] can be realized by this coating technique as well. In this context, the structuring refers to an interruption of the film in coating direction (intermittent coating) and/or rectangular to the same (stripe coating). Regarding the architecture of organic electronic devices, stripe coatings are required to enable material- and time-efficient processes. For example, for an appropriate encapsulation of an organic light emitting diode (OLED),[23,24] the coating needs to be structured between each device. For organic photovoltaics, several devices can be fabricated in one run with stripe coatings.[25,26]

In the literature, work has been done on characterizing the dominant parameters for achieving homogenous multiple stripe coatings. Numerical investigations were carried out by Wen and Liu for multiple stripes in 1995[27] in order to evaluate the effect of die design and fluid rheology on the exiting fluid flows. The most homogenous flow distribution at the outlet was achieved with a T-die and a suitable shim. Further, the influence of shim geometry on the fluid distribution has also been investigated by Han et al.[28] The shape of slit channels inside the die, which are determined by the shim itself, had the biggest influence on the fluid flow distribution. They concluded that a uniform slit channel enables the largest possible process window. Kang et al.[1] analyzed the influence of substrate velocity, gap height and flow ratio on the film stability for a simultaneous coating of two stripes. Substrate velocity was found to be the predominant parameter for controlling the coating width.

In accordance to all these works, it could be assumed that the known full-area coating defect mechanisms are transferable to stripe coating applications. Obviously, this assumption is only valid for stripes wider than the above mentioned, neck-in influenced coating edge region.

However, there is an additional upper limit in stripe coatings which is not described in the literature yet. Beyond this upper limit, the separately coated stripes tend to merge instantly during the coating application, especially if the inks are low viscous.

Therefore, the aim of this work is to reveal the mechanisms behind the upper limit in slot die stripe coating in order to establish correlations forecasting the resulting process window. To understand which parameters are influencing the onset of the upper limit, the theoretical examination will be accompanied by an experimental analysis. For each investigation, different shim geometries, two gap dimensions, several liquids with different surface tensions and viscosities were applied at a defined range of coating parameters. Defects may occur during the film deposition process as well as in the drying step where the solid film is formed. In this study, we exclusively pay attention to the coating and not the following drying step.

Materials and methods

As coating liquids, three low viscous solutions were used. All solutions are model systems which are available in large amounts. Solution I is a mixture of deionized Water and EtOH (36.6 w%). Solution II was prepared according to Wengeler et al.[29,30] adding 0.34 w% polyacrylamide (PAA) (polyacrylamide pure;

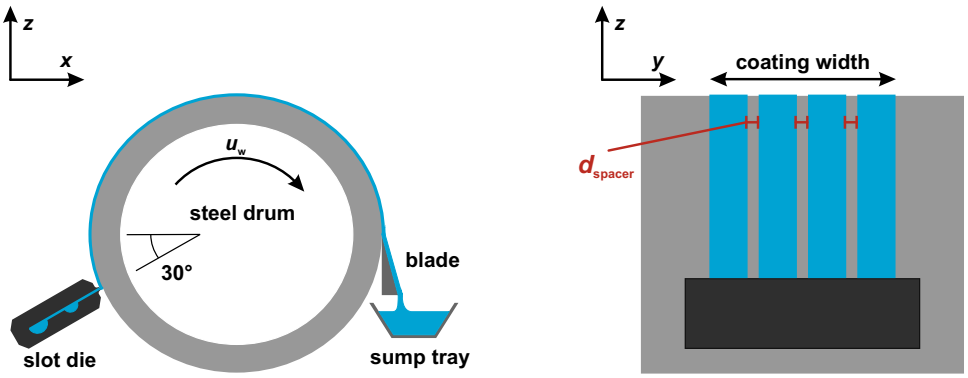

Fig. 1: Experimental setup of slot die coating on rotating steel drum (left). Schematic drawing of strip coating on steel drum (right) for the shim layout with four stripes

Table 1: Overview of shim layouts

Shim layout	Number of stripes	Coating width per stripe (mm)	Total coating width (mm)	Distance between stripes (mm)	Coating width at merging (mm)
1	4	20	80	1	84
2	4	20	80	3	92
3	4	20	80	5	100

Carl Roth GmbH + Co. KG, Karlsruhe, Germany) to deionized Water. Solution III is prepared by adding 0.1 w% of the surfactant Triton X-100 to solution II. To the solutions I to III, an amount of 0.002 w% disodium 4,4′-Bis(2-sulfonatostyryl)biphenyl (DSSB) (TCI Deutschland GmbH, Eschborn, Germany) was added as an UV-active component for visualizing issues. Surface tensions were measured with a contact angle measurement device (DSA 20 EasyDrop; Krüss, Hamburg, Germany), and rheology data were generated with a rotary rheometer (Physica MCR; Anton Paar, Graz, Austria) with a cone-plate setup. The diameter of the cone and plate was 40 mm, and the angle of the cone was 0.3° (CP40-0.3; Anton Paar, Graz, Austria).

The slot die coating setup was adjusted according to Schmitt et al.,[4,20,31] applying the slot die in 8 o'clock position on a polished chromium-plated steel drum, as shown in Fig. 1.

The two adjusted gap heights h_G measured 190 and 101 µm. The length of the down- and upstream lips l_U and l_D were 500 µm, and the shim thickness l_S and, consequently, the slot width amounted to 100 µm (see Fig. 3 as well). A slot die built in cooperation with TSE Troller AG (TSE Troller AG, Murgenthal, Switzerland) with a coating width of max. 135 mm was used with three different shim layouts shown in Table 1.

The outlet geometry of the shims was a 90 degree angle and was not modified during the experiments. All shims were made of PET with a thickness of 100 µm. For each coating solution, experiments were performed by using the three different shim layouts. The gap height was adjusted at the tightest roller to die position by using high-precision foils. The volume flow of coating solution was adjusted by using a syringe pump (Chemyx Nexus 6000, Chemyx, Stafford, USA).

The wet film was bladed off at the backside of the steel drum to enable a continuous coating process without drying step afterward. After adjusting the substrate speed of the steel drum, the volume flow was increased step by step from operation point 1–3, as schematically shown in Fig. 2.

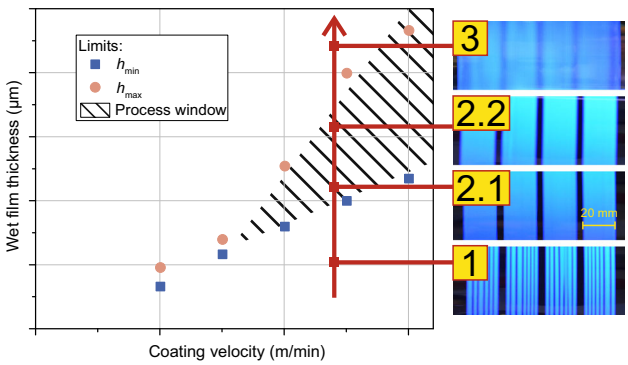

Fig. 2: Experimental procedure for the determination of the process window shown in wet film thickness h_{wet} over coating velocity u. By increasing the volume flux, one moves from point 1 until point 3 crossing the minimum wet film thickness and the upper limit for stripes. Experimental examples with shim 3 and Water–PAA solution. The lowest wet film thickness is given in blue (squares), and the merging of the stripes occurs at h_{max} (red circles) (Color figure online)

Table 2: Rheological data for coating solutions (at 20°C)

Coating solution	Viscosity				Valid range of approximation $\dot{\gamma}$ (1/s)
	At 50 1/s (mPas)	At 500 1/s (mPas)	At 5000 1/s (mPas)	Function of shear rate $\dot{\gamma}$ (mPas)	
Water–EtOH (I)	2.57	2.54	2.49	$4.1\dot{\gamma}^{-0.065}$	20–50,000
Water–PAA (II)	29.9	15.3	7.86	$93\dot{\gamma}^{-0.29}$	20–50,000
Water–PAA–Triton X (III)	31.2	15.5	7.73	$102\dot{\gamma}^{-0.303}$	20–50,000

Table 3: Static surface tension for coating solutions and their contact angle on steel (at 20°C)

Coating solution	Static surface tension (mN/m)	Standard deviation (mN/m)	Measurements (#)	Static contact angle on steel (°)
Water–EtOH (I)	32.85	0.11	4	21.9
Water–PAA (II)	71.27	0.02	6	42.9
Water–PAA–Triton X (III)	31.59	0.06	4	17.3

The coating speed and gap height were set constant for each operating point. For all applied liquids, shim and gap configurations, five coating speeds between 1 and 20 m/min were chosen. Starting each experimental trial with a low volume flow, defects were observed (point 1 in Fig. 2), which are known as rivulets from the literature.[8] As expected, the predominant defects are rivulets caused by air entrainment.[32] As described by Gutoff and Cohen,[8] the rivulets have different varieties of width. By increasing the volume flow with a step width of 0.1 ml/min, the conditions of defect-free coatings were reached (point 2.1 in Fig. 2). A coating with four homogenous stripes of 20 mm width each can be seen in picture 2.1 in Fig. 2. This point is given with blue squares in Fig. 2. To exclude unsteady effects, the observation was conducted after waiting approximately 1 m of coating. The minimum wet film thickness was obtained by calculating the average volume flow of the two operating points at the last unstable and the first stable coating conditions. A further increase in volume flow leads to an increase in stripe width (point 2.2 in Fig. 2). As expected, increasing the volume flow even further results in a spreading of the stripes until they merge inhomogeneously (point 3 in Fig. 2). As the film thickness is not evenly distributed throughout the entire coating width, the image looks blurry. It is still well focused, but no sharp edges can be observed anymore.

The conditions, when the stripes merged (red circles in Fig. 2), were tracked and chosen for analysis because the exact film and spreading widths are known at this point. Therefore, the wet film thickness can be calculated from a simple mass balance. Here, the coating width is calculated by the distance of the stripes plus four times the distance between the stripes as we assume the liquid to spread half of the given spacer width at each side of the slot die (see Table 1). To investigate the influence of the distance between the stripes, the shim layout with four stripes was modified. Three different shims providing spacing distances d_{spacer} of 1, 3 and 5 mm (Shim 1, 2, 3 in Table 1) between the stripes were manufactured and used for the experiments. The merging of the stripes is investigated with fluid formulations I, II and III. While solutions I and II have similar surface tensions, II and III have similar viscosities. This provides the ability to distinguish between the influence of liquid characteristics on the gained results.

The obtained data of the five coating fluid viscosities are shown in Table 2. The viscosity was fitted according to a power law approach for the relevant interval of shear rates. Coating liquid I shows almost Newtonian behavior, whereas solutions II and III are shear thinning. The shear thinning behavior of II and III and their absolute values are often observed for organic photovoltaic applications.[29]

The values of surface tension for I and III are quite low in a range of $\sim$ 30 mN/m. Solution II has almost the same surface tension as Water with 71.9 mN/m. The data of the surface tension are summed up in Table 3.

Results and discussion

Determination of process window

The following section is supposed to build a basis for the investigation and definition of a potential upper coating limit. Therefore, the on-hand theoretical process window, defining the lower limit, will be discussed and compared to the experimental results.

To obtain a uniform and closed film, a stable coating bead is required. The coating bead pressure gradient Δp_{DU} in coating direction can be calculated by the sum of multiple pressure drops[12] (compare Fig. 3). Regarding the minimal, expectable film thickness before air

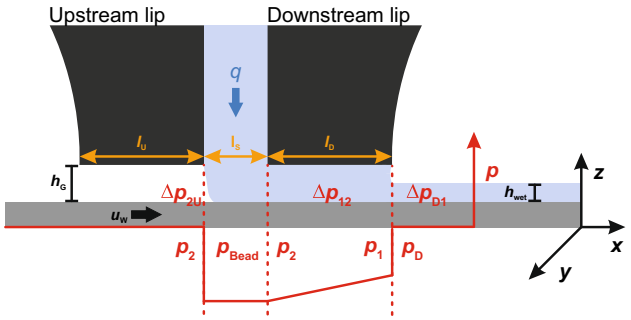

Fig. 3: Schematic drawing of slot die gap with the relevant bead pressures

breaks through the coating bead, the upstream meniscus is supposed to be pinned at the inner corner of the upstream lip corresponding to case 4 as presented by Higgins and Scriven in 1980[32] and discussed by Durst and Wagner[34] as well as Schmitt[20] in more detail. In this context, the coating bead pressure drop Δp_{DU} can be described by equation (1) including the pressure drop of the downstream meniscus Δp_{D1}, the downstream gap Δp_{12}, and the upstream meniscus Δp_{2U}.

$$\Delta p_{DU} = \Delta p_{D1} + \Delta p_{12} + \Delta p_{2U} \tag{1}$$

Following the above power law approach for non-Newtonian liquids, these pressure drops are given by:

$$\Delta p_{D1} = 1.34 \mathrm{Ca}^{\frac{2}{3}} \frac{\sigma}{h_{\mathrm{wet}}} \tag{2}$$

With the capillary number Ca defined as

$$\mathrm{Ca} = \kappa \frac{u_{\mathrm{W}}^{n}}{\sigma \cdot h_{\mathrm{G}}^{n-1}} \tag{3}$$

As well as the downstream pressure drop Δp_{12} derived from Lee et al.[20,33]:

$$\Delta p_{12} = -l_{\mathrm{D}} \cdot \kappa \cdot \left(\frac{(n+1)(2n+1)}{n} \right)^{n} \cdot \frac{(2 \cdot h_{\mathrm{wet}} - h_{\mathrm{G}})^{n}}{h_{\mathrm{G}}^{(2n+1)}} \cdot u_{\mathrm{W}}^{n} \quad \text{For } h_{\mathrm{wet}} > h_{\mathrm{G}}/2 \tag{4.1}$$

$$\Delta p_{12} = l_{\mathrm{D}} \cdot \kappa \cdot \left(\frac{(n+1)(2n+1)}{n} \right)^{n} \cdot \frac{(2 \cdot h_{\mathrm{wet}} - h_{\mathrm{G}})^{n}}{h_{\mathrm{G}}^{(2n+1)}} \cdot u_{\mathrm{W}}^{n} \quad \text{For } h_{\mathrm{wet}} < h_{\mathrm{G}}/2 \tag{4.2}$$

And the capillary pressure gradient Δp_{2U} which considers the wettability of the lips and the moving web[32]

$$\Delta p_{2U} = -\frac{2\sigma}{h_{\mathrm{G}}} (\cos\vartheta + \cos\theta) \tag{5}$$

The static contact angle θ of each coating solution on steel was experimentally determined and is listed in Table 3 in the experimental section. The dynamic contact angle ϑ is calculated by[6,35]

$$\vartheta = 73 \cdot u_{\mathrm{w}}^{0.22} \cdot \eta^{0.18} \cdot \sigma^{0.11} \tag{6}$$

To determine the minimum film thickness, a failure of the upstream meniscus, indicated by air entrainment, must be avoided. Thus, the pressure gradient [equation (1)] has to equal 0 when ambient coating conditions are applied. As proposed by Schmitt,[20] the minimal wet film thickness is calculated by solving the implicit pressure balance as a function of the coating velocity after employing equations (2)–(6) and a comparison with the experimental data is added.

Moving on to the experimental results, the results for a gap width of 190 µm are shown and discussed in this part, while the figures for gap widths of 101 µm are given in the supporting information since they show similar tendencies. Since Figs. 4, 5, and 6 show a similar general structure, a brief explanation is given: The minimum wet film thickness h_{min} and the maximum wet film thickness h_{max} (merging of the stripes) are depicted for the three shim layouts; the former indicated as open black squares, the latter as diamonds (1 mm spacer), circles (3 mm spacer), and triangles (5 mm spacer). The theoretically calculated film thickness given as dashed line is compared with the experimentally observed lower limits. For the mini-

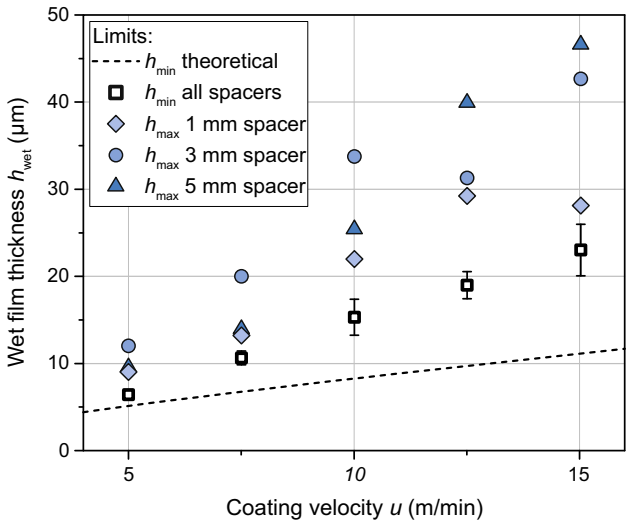

Fig. 4: Process window of Water–EtOH (I) for a gap width of 190 µm. Calculated theoretical minimum wet film thickness according to equation (1) is given as dashed line. Experimentally determined minimum wet film thickness is shown as black open squares with error bars. Diamonds (light blue) correspond to the upper coating limit of shim 1, circles (medium blue) are the results for a spacer width of 3 mm, and triangles (dark blue) symbolize the spacer width of 5 mm (Color figure online)

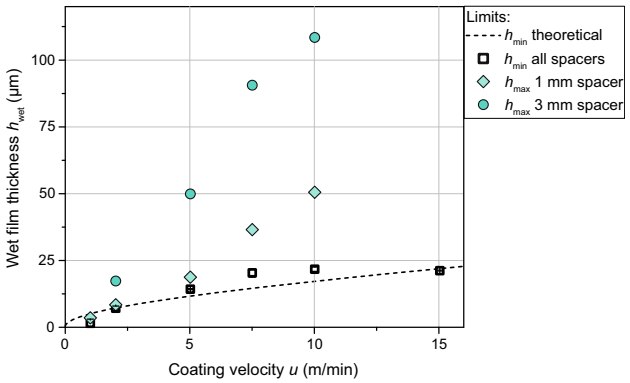

Fig. 5: Process window for Water–PAA(II) for a gap width of 190 µm. Calculated theoretical minimum wet film thickness according to equation (1) is given as dashed line. Experimentally determined minimum wet film thickness is given as black open squares with error bars. Diamonds (light green) correspond to the upper coating limit for shim 1, and circles (medium green) are the results for a spacer width of 3 mm (Color figure online)

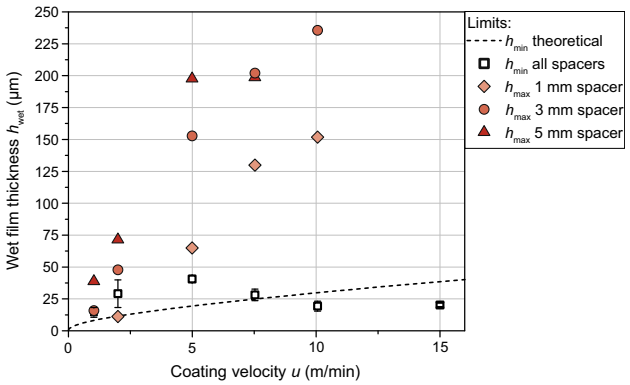

Fig. 6: Process window for Water–PAA–Triton X (III) for a gap width of 190 µm. Calculated theoretical minimum wet film thickness according to equation (1) is given as dashed line. Experimentally determined minimum wet film thickness is given as black open squares with error bars. Diamonds (light red) correspond to the upper coating limit for shim 1, circles (medium red) are the results for a spacer width of 3 mm, and triangles (dark red) symbolize the spacer width of 5 mm (Color figure online)

mum wet film thickness, the average of all measurements conducted with the different shim layouts is taken together as we assume that the shim geometry does not affect the minimum wet film thickness. Error bars indicate the deviation between the measured minimum wet film thickness for the different shims. As it will be shown, the error bars are low and therefore they confirm the hypothesis that the minimum wet film thickness is independent of the shim geometry. The process window is located between the minimum wet film thickness for all spacers and the maximum wet film thickness for each spacer, as demonstrated in principle in Fig. 2. The results for Water–EtOH (I) are shown in blue, Water–PAA (II) is colored in green, and red represents the coating window of the coating solution Water–PAA–Triton X (III).

In Fig. 4, the results for Water–EtOH (I) with a gap width of 190 µm are illustrated.

Comparing the calculations and the experimental findings for the minimal wet film thickness, the observed values are higher than the calculated ones. These deviations may occur due to limited accuracy in the roller bearing,[20] in adjusting the coating gap, the volume flux, and the coating velocity. For all coating velocities, standard deviations for the minimum wet film thickness are small compared to the absolute values, which state that the minimum wet film thickness is independent of the used shim geometry. With increasing coating velocity, the minimum wet film thickness (experimental observations and calculations) increases. As expected due to inertia forces, the maximum wet film thickness until merging increases with increasing coating velocity as well. For low coating speeds, no difference in minimum and maximum wet film thicknesses can be observed. For the coating solution Water–EtOH, it can be stated that stripes without defects cannot be applied at coating speeds under 5 m/min at ambient conditions. As the spacer width increases, the process window for stripe coating gets larger with rising coating velocity. This is illustrated by the increase in maximum wet film thickness by the circles and diamonds corresponding to shim layouts 2 and 3 (see spacer width 3 mm and 5 mm in Fig. 4). Even though this observation—thicker films with larger spacer width before merging—does not apply for all employed coating speeds, this general tendency can be seen clearly.

In Fig. 5, the results for the second investigated coating solution Water–PAA (II) are shown for the gap width of 190 µm. Theoretically determined and experimentally measured minimum wet film thicknesses differ only slightly. For each coating velocity, the maximum wet film thickness is higher for the shim layout with 3 mm spacer compared to the one with 1 mm spacer. No merging of the stripes was observed for the shim geometry with a spacer width of 5 mm until the maximum volume flow possible with the used syringe pump (300 ml/min) was reached. Comparing the result of coating solution II (Fig. 5) with I (Fig. 4), the required minimum wet film thickness h_{min} is about twice as high as the one for Water–EtOH, the fluid with the lower viscosity. At the same time, the considerably higher maximum wet film thicknesses are possible, finally resulting in a much larger process window. For the coating velocity of 15 m/min, no merging of the stripes was observed either. Considering slower coating speeds, the process window for the coating of stripes can be extended to speeds down to 2.5 m/min. For coating speeds close to 2.5 m/min, the process window does not allow a great variation of the wet film thickness as defect-free coatings are soon followed by merging of the stripes when increasing the wet film thickness.

The results for the third studied coating solution Water–PAA–Triton X (III) are given in Fig. 6. For Water–PAA–Triton X (III), the highest minimum wet film thicknesses were calculated and observed in the experiments compared to the remaining ones. Likewise Water–PAA (II), the calculated and experimentally determined minima differ only slightly from each other. Regarding the process window for stripe coatings, the largest coating windows were observed for Water–PAA–Triton X. Wet film thicknesses of more than 100 µm are possible even for lower coating velocities. At 10 m/min, no merging of the stripes is observed for the shim layout with spacer width of 5 mm and at 15 m/min the stripes are stable for all spacer widths up to wet film thicknesses of more than 250 µm. While there is a significant difference of the maximum wet film thickness between 1 and 3 mm spacer width, the difference between the shims with 3-mm and 5-mm spacer width is rather small. Nonetheless, the tendency that for larger spacer width the process window increases can be confirmed. Similar to the findings of Water–PAA, stripes can already be coated at 2.5 m/min as there is a slight difference between minimum and maximum wet film thicknesses. At a coating speed of 10 m/min three times thicker wet films can be applied with Water–PAA when adding Triton X (150 µm) compared to Water–PAA without surfactant (50 µm). The wetting agent Triton X and the resulting reduced surface tension seem to have a positive effect on the upper limit. This increases the area of the stable coating in the process window.

Comparing Figs. 4, 5, and 6 in regard to the minimum wet film thickness, one has to keep in mind the different scales for the film thickness. In absolute values, the minimum wet film thickness is deviating from the prediction in a similar amount. However, the underestimation for Water–EtOH seems to be with continuity compared to the Water–PAA solutions. We assume that, on the one hand, a higher gap width which is due to the roller's bearing inaccuracy causes an underestimation of the minimum wet film thickness in general, while the absence of a vacuum chamber on the other hand causes a unpinned, mobile coating bead, which is prone to disturbances, especially for higher viscosities as observed for the Water–PAA solutions. When comparing Figs. 4 and 6, the primary influence of viscosity can be investigated, while comparing Figs. 5 and 6 gives a hint toward the influence of surface tension. As the process window is the largest for Fig. 6, a higher viscosity and a lower surface tension seem to be beneficial in terms of process stability. If very thin films are required, Water–EtOH with a very low viscosity is to be favored.

Finally, the following observations for stripe coatings can be stated

- An increasing spacer width d_{spacer} increases the process window
- A lower gap height h_{Gap} leads to similar process windows (see Figures SI1, SI2, SI3 in supplementary information). For smaller gap heights, the dependency of the process window on the spacer width is larger.
- For coating speeds lower than 2.5 m/min, no stable process conditions can be found for defined stripe coatings.

For the chosen process windows, the influence of viscosity η, surface tension σ, film height h_{wet}, and web speed u_{W} on the maximum film thickness $h_{\max}$ is discussed in the next part. In summary, higher viscosities and surface tensions as well as higher coating speeds are favored to obtain a larger process window.

A first theoretical approach to explain the experimental findings and an upper limit for stripe coatings

To describe the spreading and explain the observed upper limit $h_{\max}$ for stripe coating, an expression describing the pressure situation at the side of the coating bead(s) has to be determined. Obviously, the bead reaches the widest spreading width where the bead pressure reaches a maximum. In usual operation, the highest bead pressure is reached along the feed slot, assuming a constant pressure level for this area, independently of x- and y-direction. As described above, the pressure gradient in the slot is described by individual pressure drops[12] and the dynamic coating bead pressure p_{Bead} can be derived from equation (1) by

$$p_{\text{Bead}} = p_D - \Delta p_{D1} - \Delta p_{12} \tag{7}$$

In cross-web direction, the pressure drop between the bead p_{Bead} and the applied surrounding conditions p_{Vac} can be described by an unknown pressure drop Δp_{Side} toward the side and capillary forces. We assume that this balancing is done by the capillary pressure of the menisci Δp_{Cap} and compensated by yet an unknown pressure gradient Δp_{Side} along the wetted side gaps and the bead pressure (see Fig. 7).

$$p_{\text{Vac}} - p_{\text{Bead}} = \Delta p_{\text{Side}} + \Delta p_{\text{Cap}} \tag{8}$$

With $\Delta p_{Side} = p_{2-}p_3$.

In Fig. 7, the assumed pressure distribution underneath the side gap, rectangular to the coating direction, is drawn schematically.

Due to the premetered nature of the slot die coating method, the conditions are equal at all side-warded wetting lines. Therefore, it is not necessary to differentiate between the individual wetting lines of a striped coating or a single-film coating. As we do not apply any

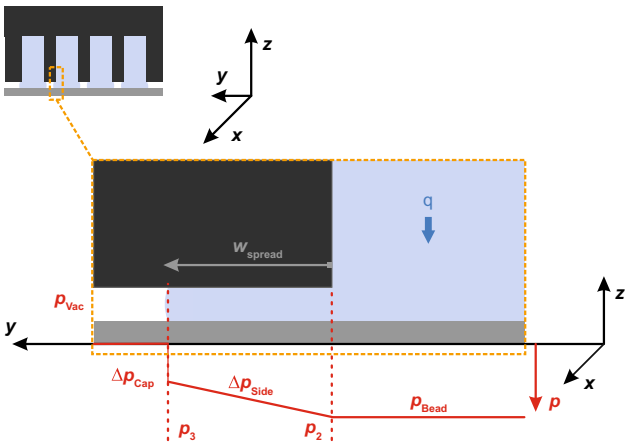

Fig. 7: Schematic drawing of the assumed pressure distribution underneath the side gap of a slot die in cross-web direction with shim layout 3. The figure shows an operating point at which the stripe width is enlarged

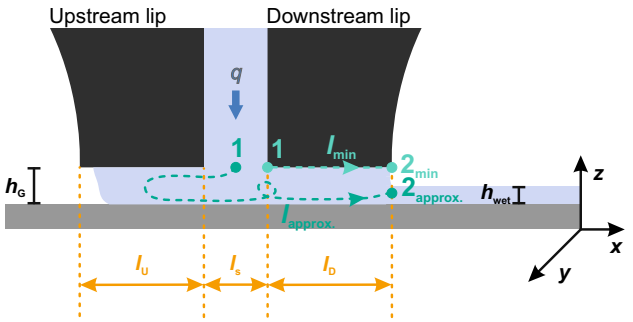

Fig. 8: Schematic drawing of slot die gap illustrating the two assumed ways from 1 to 2 for a tracked particle in the fluid flow which moves in the coating bead in *x*- and *y*-direction. L_{min} illustrates the shortest possible distance for the tracked particle, and $l_{approx.}$ is required to lead the correct pressure balance in equation (9)

vacuum and p_{Vac} equals p_D, both pressures can be crossed out and the relation above can be simplified to:

$$\Delta p_{Bead} = \Delta p_{Side} + \Delta p_{Cap} \tag{9}$$

With $\Delta p_{Bead} = \Delta p_{D1} + \Delta p_{12}$.

The side-warded meniscus is assumed to generate a capillary pressure drop Δp_{Cap} based on the contact angles of the coating liquids on the chromium-plated steel drum (see Table 3). For the calculation of Δp_{Cap}, the equation for dynamic capillary pressure drop is applied comparable to the pressure balance in coating direction but with a positive sign [compare equations (5), and (6)]. Since we aim to describe the merging point which indicates the maximal achievable film thickness, the capillary pressure and the side-warding pressure were considered to compensate p_{Bead}. In our first approach, we postulate a convex shaped meniscus since the pressure of the spreading fluid in the side gap has to push the menisci toward the sides against the capillary forces and reaches its maximum at the merging point.

Furthermore, by using the approximation for the dynamic contact angle [see equation (6)], we assume a dynamic contact angle in cross-web direction which is mainly controlled by forces that occur in web direction since there is yet no description for side-warded dynamic contact angle available. However, by slightly changing its shape, the meniscus might also dampen changes in bead pressure before spreading of the new surface occurs.

Regarding equations (8), and (9), respectively, the pressure gradient Δp_{Side} is still unknown. If the applied conditions change, Δp_{Side} will react via the spreading width w_{Spread} and toward higher flow rates or lower web speeds, the spreading width will increase. Thus, an acceptable spreading width defines the upper limit in the slot die process window. Here we define the merging of the stripes as the point which cannot be tolerated any longer. Spreading will occur if the bead pressure drop Δp_{Bead} cannot be balanced by Δp_{Cap} and Δp_{Side} anymore as given by equation (10).

$$p_{Bead} > \Delta p_{Side} + \Delta p_{Cap} \tag{10}$$

For the prediction of the upper limit, an equation of the unknown pressure gradient Δp_{Side} including the spreading width w_{Spread} is needed. Therefore, we start with the assumption that the specific volume flux is composed of a mixture of a Hagen–Poiseuille flow (considering the pressure-driven flow toward the sides) and Couette flow [describing the moving wall-induced flow, orthogonal to the cross section; see equation (11)] following the analytic description of pressure distribution in the coating bead in web direction. This consideration is a first simplified approach to approximate the unknown fluid flow distribution.

$$\begin{aligned} q &= q_{Couette} - q_{Hagen-Poiseuille} \\ &= \frac{u_{y,Fluid} \cdot h_G}{2} - \frac{h_G^3}{12 \cdot \eta} \cdot \frac{dp_y}{dy} \end{aligned} \tag{11}$$

Here, the pressure gradient $\frac{dp_y}{dy}$ describes the existing pressure drop in cross-web direction, between 2 and 3 in Fig. 7. In a next step, we set equation (11) to 0 as the total volume flux toward the sides equals zero at stationary coating conditions: The same amount of fluid entering the side gap is supposed to leave at constant spread width. Proceeding with this postulate and neglecting flow-field implied viscosity changes for non-Newtonian liquids, equation (11) can be transformed, integrated, and rewritten by

$$\Delta y_{32} = y_3 - y_2 = \frac{h_G^2}{6 \cdot \eta \cdot u_{y,Fluid}} \cdot \Delta p_{32} \tag{12}$$

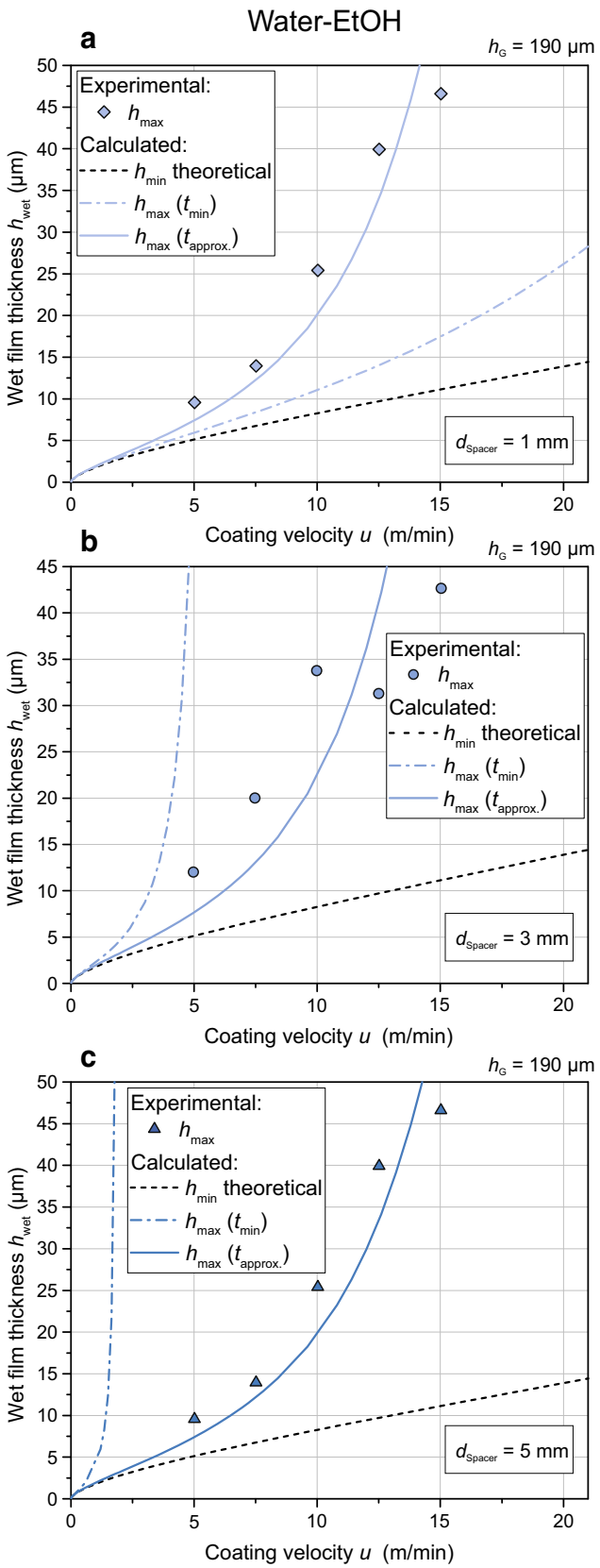

◀Fig. 9: Calculation of the upper limit of Water–EtOH determined for t_{min} (dashed lines) and $t_{approx.}$ (solid lines) compared with experimental observed upper limit (symbols) and the calculated lower limit (black dotted lines): the wet film thickness is plotted as a function of the coating velocity at a gap width of 190 µm for the three different spacer distances of 1 mm (a), 3 mm (b), and 5 mm (c)

The velocity, the fluid spreads with, is expressed by

$$u_{y,\mathrm{Fluid}} = \frac{\Delta y_{32}}{t_{\mathrm{spread}}} \tag{13}$$

where Δy_{32} corresponds to w_{spread} (compare Fig. 7) and t_{spread} is the spreading time. Combining equations (12), and (13) results in an expression of w_{spread} as function of the unknown pressure drop $\Delta p_{32} = p_3 - p_2$

$$w_{\mathrm{spread}} = \Delta y_{32} = h_{\mathrm{G}} \sqrt{\frac{t_{\mathrm{spread}}}{6 \cdot \eta} \cdot \Delta p_{32}} \tag{14}$$

At the merging point, w_{spread} measures 0.5 times the spacer width d_{Spacer} and an equation can be derived for Δp_{Side} by rewriting equation (14) as follows:

$$\Delta p_{\mathrm{Side}} = -\Delta p_{32} = -\frac{6\eta}{t_{\mathrm{spread}}} \cdot \left(\frac{d_{\mathrm{Spacer}}}{2h_{\mathrm{G}}}\right)^2 \tag{15}$$

With $\Delta p_{\mathrm{Side}} = p_2 - p_3$. Note that the signs of Δp_{Side} and Δp_{32} are reversed due to the direction of integration.

With regard to equation (15), the only unknown parameter is t_{spread}. The time, a tracer particle has for spreading in cross-web direction, is mainly controlled by the coating velocity and the distance it moves through the coating bead in x-direction. To enable comparison with observations in the experiments, we assume that the merging occurs the latest directly at the end of the downstream lip. Thus, we approximate the time by

$$t_{\mathrm{spread}} = \frac{l_x}{u_{\mathrm{W}}} \tag{16}$$

Since the travelled distance of a molecule in the coating solution is not available, we estimate it via two different methods:

In the first one, we assume the shortest path the molecule could take (compare l_{min} in Fig. 8) and calculate the minimal spreading time t_{min} [see equation (17)].

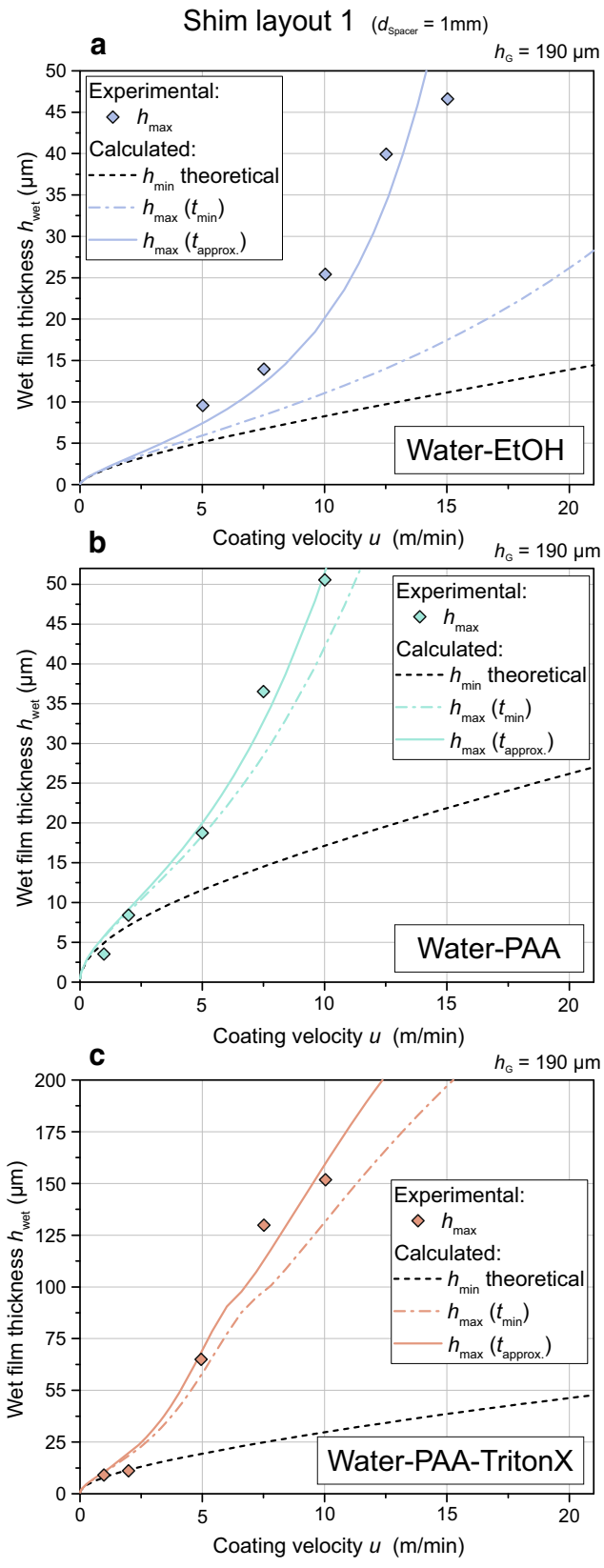

◀Fig. 10: Calculation of the upper limit of different coating solutions determined for t_{min} (dashed lines) and $t_{approx.}$ (solid lines) compared with experimental observed upper limit (symbols) and the calculated lower limit (black dotted lines): the wet film thickness is plotted as a function of the coating velocity at a gap width of 190 µm and constant spacer distance of 1 mm for the three different solutions Water–EtOH (a), Water–PAA (b), and Water–PAA–Triton X (c)

$$t_{\min} = \frac{l_D}{u_W} \tag{17}$$

Finally, the implicit pressure balance in y-direction can be solved by calculating the maximum film thickness $h_{max}(t_{min})$ for the assumed minimal spreading time t_{min} as function of the coating velocity. To do so, we apply equations (7), (15), (16), and (17) to the expression of the pressure balance [equation (9)] to determine the upper limit h_{max} at which merging takes place.

Moving on to our second approach, we determine an approximated time $t_{approx.}$ by adding a correction factor (CF) and fitting it to our experimental data. Since it is difficult to forecast the way the molecule might take without detailed knowledge about the three-dimensional flow field, we define a hypothetic path l_{approx} (refer to Fig. 8) and apply the correction factor (CF) to t_{approx} [see equations (18), and (19)]. Note that for the determination of $h_{max}(t_{min})$, the correction factor CF is set to 1.

$$t_{approx.} = \frac{\frac{1}{CF} \cdot \left(\frac{l_S + h_g}{2} + l_D\right)}{u_W} \tag{18}$$

$$\Delta p_{Side} = -\Delta p_{32} = -CF \cdot \frac{6\eta}{t_{spread}} \cdot \left(\frac{d_{Spacer}}{2h_G}\right)^2 \tag{19}$$

Here, $h_{max}(t_{approx})$ is calculated by again solving the implicit pressure balance [equation (9)] with applied equations (7), (16), (18), and (19), while simultaneously the correction factor CF is adjusted to obtain the best approximation of the experimental data.

Upper limit and maximum h_{wet} film thickness calculations

In Figs. 9 and 10, the results for the calculated maximum wet film thickness $h_{max}(t_{min})$ and $h_{max}(t_{approx})$ as well as the theoretically determined minimum wet film thickness h_{min} are shown. Additionally, the experimental values for the maximum wet film thickness are given with the corresponding symbols according to the nomenclature of the previous sec-

Table 4: Overview of the adjusted correction factors CF and approximated travel distance $l_{approx.}$ for all investigated coating solutions, shim layouts, and gap width

Coating solution	Gap width (μm)	Shim layout (#)	Spacer width (mm)	CF	Travel distance (mm)
Water–EtOH (I)	190	1	1	5.90	0.111
Water–EtOH (I)	190	2	3	0.70	0.921
Water–EtOH (I)	190	3	5	0.23	2.804
Water–PAA (II)	190	1	1	2.50	0.258
Water–PAA–Triton X (III)	190	1	1	2.40	0.269

For all calculation, the minimal travel distance l_{min} equals the length of the downstream lip which measures l_D = 500 μm

tion. The results are discussed exemplarily with the findings for Water–EtOH for the gap width of 190 μm with different spacer widths (Fig. 9) and a comparison of the three different coating solutions is shown for the spacer width of 1 mm and the gap width of 190 μm in Fig. 10.

Referring to the minimum wet film thickness in Figs. 9a, 9b, and 9c, the values are the same as presented in the previous section (see Fig. 4). Calculating the upper limit with the minimal distance l_{min} for a hypothetically tracked particle, the maximum possible wet film thickness $h_{max}(t_{min})$ is underestimated for a spacer distance of 1 mm (Fig. 9a). As the spacer distance is increased (Figs. 9b and 9c), the usage of l_{min} results in an overestimated maximum possible wet film thickness. Transferring that into the time, the particle remains in the bead, and the actual time should even be shorter according to our proposed model (compare Fig. 9a), which seem to be almost impossible. For the spacer width of 3 and 5 mm, the distance which the particle travels in reality has to be much larger as demonstrated by the correction factor of the fit. All correction factors (CF), which have been applied to obtain the best approximation of the experimental data, are given in Table 4 for the combinations shown in the manuscript and for all conducted experiments in the SI Table SI1. Interpreting the values of CF, a factor larger than 1 means that the distance or time the tracer particle should have travelled is smaller than assumed by l_{min}. For values of CF smaller than 1, the travelled distance is larger than the minimal distance. In Table 4, the trend of smaller CF values with increasing spacer width can be observed. This is expected as a larger spacer width obviously enables higher maximum wet film thicknesses (see Figs. 4, 5, and 6). By adjusting CF in Figs. 9a, 9b, and 9c, the fit of h_{max} describes the upper limit for the merging of the stripes quite well.

When having a closer look at the next figure, Fig. 10a shows the same data as Fig. 9a to facilitate a comparison of the three applied coating solutions which are shown in Figs. 10b and 10c. The upper limits of all investigated systems are exemplarily depicted at a gap width of 190 μm and a spacer width of 1 mm (see Figures SI4-8 in supplementary information for the sake of completeness). As already stated for the Water–EtOH system (Fig. 9a and 10a), our proposed model overestimates the calculated minimum residence time for a spacer width of 1 mm. However, considering the coating solutions II, Water–PAA (Fig. 10b), and III, Water–PAA–Triton X (Fig. 10c), respectively, the calculated upper limits $h_{max}(t_{min})$ for the minimum residence time and the experimentally determined limits are in good agreement. This indicates that higher viscous systems are more consistent with the initial model when comparing shim layout 1. However, this observation cannot be stated for the results with a larger spacer width (see Figures SI4-8 in the supplementary information).

For Water–PAA (Fig. 10b), the approximation with the correction factor CF is smooth, while the fit for Water–PAA–Triton X (Fig. 10c) is not that straight. Attention has to be drawn that the scale has been adjusted for Fig. 10c due to the larger process window resulting in much higher wet film thicknesses. Accordingly but not displayed here, the model results in a slight curvature at higher thickness ranges for coating solutions I and II as well. As already noted for the comparison of Figs. 5 and 6, the addition of the wetting agent Triton X increases the calculated minimum wet film thickness. The upper limit of the stripe coating is shifted toward higher wet film thickness. Referring to the findings in Figs. 9 and 10 as well as Table 4, it is obvious that the model requires further improvements to predict the upper limits based on process and material data. An important information, which is missing in order to improve the model, is the precise determination of the length of the wetted upstream lip section for a more precise estimation of the traveled distance of the tracer particle. To overcome this missing information, correction factors were added to the initial model to enlarge or shorten the travelled tracer particle distance. The low correction factors for solutions II and III imply that the accuracy of the model increases with the solutions viscosity. However, according to the derivation of the model, only Newtonian fluids should be described accurately. The model does not distinguish between the different shear forces in x- and y-direction, which leads to uncertainties in the calculated viscosities.

Conclusion and outlook

Slot die coating is one of the prevailing film deposition methods for high-precision thin-film applications. For industrial purposes, the process windows of this method are of major interest. In this work, we compared the coating limit models available for large area coatings with experimental results in stripe coating applications with attention to low viscosities. It could be shown that air entrainment-induced film breakup determines the minimum wet film thickness in the coatings.

As expected, experimental observations on striped slot die coating showed that thick films limit the process window due to merging stripes. It was shown that decreasing the gap height did not significantly affect the process window. For higher spacer widths between the stripes, a larger process window was observed as well. The influence of material properties stated that surface tension is more important than viscosity and that an increase in viscosity and decrease in surface tension were favorable to obtain larger process windows.

Additionally, a model for an upper limit for striped slot die coating was suggested. In a first approach, a side pressure drop was identified to be balancing the coating bead pressure and the capillary pressure underneath the sides of the coating gap. A suggestion for the composition of the side pressure drop in cross-web direction was made and compared to the experimental observations. By the implementation of a correction factor for describing unknown flow conditions, it was possible to describe the upper coating limit for the applied liquids and the given parameter sets quite well.

Our future work focuses on further improvement of the model as well as experimental determination of pressure drops and the observation of the wetting of the die lips.

Acknowledgments The authors acknowledge financial support via the projects KOBALT and POESIE of the German Federal Ministry of Education and Research (Contract Nos. 13N0883 and 13N13692) and Philips Technologie GmbH Innovative Technologies, Aachen. We would like to thank all involved mechanics, assistants, and students for contributing to this work as well as TSE Troller AG, Murgenthal, Switzerland, for technical support.

References

1. Kang, H, Park, J, Shin, K, ''Statistical Analysis for the Manufacturing of Multi-strip Patterns by Roll-to-Roll Single Slot-Die Systems.'' *Robot. Comput. Integr. Manuf.*, **30** (4) 363–368 (2014)
2. Peters, K, Wengeler, L, Scharfer, P, Schabel, W, ''Liquid Film Coating of Small Molecule OLEDs.'' *J. Coat. Technol. Res.*, **11** (1) 75–81 (2014)
3. Krebs, FC, ''Fabrication and Processing of Polymer Solar Cells. A Review of Printing and Coating Techniques.'' *Solar Energy Mater. Solar Cells*, **93** (4) 394–412 (2009)
4. Schmitt, M, Scharfer, P, Schabel, W, ''Slot Die Coating of Lithium–Ion Battery Electrodes: Investigations on Edge Effect Issues for Stripe and Pattern Coatings.'' *J. Coat. Technol. Res.*, **11** (1) 57–63 (2014)
5. Schmitt, M, Diehm, R, Scharfer, P, Schabel, W, ''An Experimental and Analytical Study on Intermittent Slot Die Coating of Viscoelastic Battery Slurries.'' *J. Coat. Technol. Res.*, **12** (5) 927–938 (2015)
6. Kistler, SF, Schweizer, PM (eds.), *Liquid Film Coating*. Springer, Dordrecht, 1997
7. Tsuda, T, ''Coating Flows of Power-Law Non-Newtonian Fluids in Slot Coating.'' *J. Soc. Rheol. Jpn.*, **38** (4/5) 223–230 (2010)
8. Gutoff, EB, Cohen, ED, Kheboian, GI, *Coating and Drying Defects: Troubleshooting Operating Problems*. Wiley-Interscience, Hoboken (2006)
9. Romero, OJ, Carvalho, MS, ''Response of Slot Coating Flows to Periodic Disturbances.'' *Chem. Eng. Sci.*, **63** (8) 2161–2173 (2008)
10. Ruschak, KJ, ''Limiting Flow in a Pre-metered Coating Device.'' *Chem. Eng. Sci.*, **31** 1057–1060 (1976)
11. Carvalho, MS, Kheshgi, HS, ''Low-Flow Limit in Slot Coating: Theory and Experiments.'' *AIChE J.*, **46** (10) 1907–1917 (2000)
12. Schmitt, M, Raupp, S, Wagner, D, Scharfer, P, Schabel, W, ''Analytical Determination of Process Windows for Bilayer Slot Die Coating.'' *J. Coat. Technol. Res.*, **12** (5) 877–887 (2015)
13. Dobroth, T, Erwin, L, ''Causes of Edge Beads in Cast Films.'' *Polym. Eng. Sci.*, **26** (7) 462–467 (1986)
14. Abbel, R, de Vries, I, Langen, A, Kirchner, G, t'Mannetje, H, Gorter, H, Wilson, J, Groen, P, ''Toward High Volume Solution Based Roll-to-Roll Processing of OLEDs.'' *J. Mater. Res.*, **32** (12) 2219–2229 (2017)
15. Raupp, S, Daume, D, Tekoglu, S, Merklein, L, Lemmer, U, Hernandez-Sosa, G, Sauer, HM, Dörsam, E, Scharfer, P, Schabel, W, ''Slot Die Coated and Flexo Printed Highly Efficient SMOLEDs.'' *Adv. Mater. Technol.*, **2** 1600230 (2017)
16. Raupp, SM, Merklein, L, Hietzschold, S, Zürn, M, Scharfer, P, Schabel, W, ''Slot Die-Coated Blue SMOLED Multilayers.'' *J. Coat. Technol. Res.*, **14** (5) 1029–1037 (2017)
17. Raupp, SM, Merklein, L, Pathak, M, Scharfer, P, Schabel, W, ''An Experimental Study on the Reproducibility of Different Multilayer OLED Materials Processed by Slot Die Coating.'' *Chem. Eng. Sci.*, **160** 113–120 (2017)
18. Choi, K-J, Lee, J-Y, Shin, D-K, Park, J, ''Investigation on Slot-Die Coating of Hybrid Material Structure for OLED Lightings.'' *J. Phys. Chem. Solids*, **95** 119–128 (2016)
19. Choi, K-J, Lee, J-Y, Park, J, Seo, Y-S, ''Multilayer Slot-Die Coating of Large-Area Organic Light-Emitting Diodes.'' *Org. Electron.*, **26** 66–74 (2015)
20. Schmitt, M, *Slot Die Coating Of Lithium–Ion Battery Electrodes*. KIT Scientific Publishing, Karlsruhe, 2016
21. Søndergaard, RR, Hösel, M, Krebs, FC, ''Roll-to-Roll Fabrication of Large Area Functional Organic Materials.'' *J. Polym. Sci. B Polym. Phys.*, **51** (1) 16–34 (2013)
22. Hong, S, Lee, J, Kang, H, Lee, K, ''Slot-Die Coating Parameters of the Low-Viscosity Bulk-Heterojunction Materials Used for Polymer Solarcells.'' *Solar Energy Mater. Solar Cells*, **112** 27–35 (2013)

23. Cho, AR, Kim, EH, Park, SY, Park, LS, ''Flexible OLED Encapsulated with Gas Barrier Film and Adhesive Gasket.'' *Synth. Met.*, **193** 77–80 (2014)
24. Park, J-S, Chae, H, Chung, HK, Lee, SI, ''Thin Film Encapsulation for Flexible AM-OLED. A Review.'' *Semicond. Sci. Technol.*, **26** (3) 34001 (2011)
25. Hösel, M, Søndergaard, RR, Jørgensen, M, Krebs, FC, ''Fast Inline Roll-to-Roll Printing for Indium-Tin-Oxide-Free Polymer Solar Cells Using Automatic Registration.'' *Energy Technol.*, **1** (1) 102–107 (2013)
26. Andersen, TR, Cooling, NA, Almyahi, F, Hart, AS, Nicolaidis, NC, Feron, K, Noori, M, Vaughan, B, Griffith, MJ, Belcher, WJ, Dastoor, PC, ''Fully Roll-to-Roll Prepared Organic Solar Cells in Normal Geometry with a Sputter-Coated Aluminium Top-Electrode.'' *Solar Energy Mater. Solar Cells*, **149** 103–109 (2016)
27. Wen, S-H, Liu, T-J, ''Extrusion Die Design for Multiple Stripes.'' *Polym. Eng. Sci.*, **9** (35) 759–767 (1995)
28. Han, GH, Lee, SH, Ahn, W-G, Nam, J, Jung, HW, ''Effect of Shim Configuration on Flow Dynamics and Operability Windows in Stripe Slot Coating Process.'' *J. Coat. Technol. Res.*, **11** (1) 19–29 (2014)
29. Wengeler, L, Peters, K, Schmitt, M, Wenz, T, Scharfer, P, Schabel, W, ''Fluid-Dynamic Properties and Wetting Behavior of Coating Inks for Roll-to-Roll Production of Polymer-Based Solar Cells.'' *J. Coat. Technol. Res.*, **11** (1) 65–73 (2014)
30. Wengeler, L, Schmitt, M, Peters, K, Scharfer, P, Schabel, W, ''Comparison of Large Scale Coating Techniques for Organic and Hybrid Films in Polymer Based Solar Cells.'' *Chem. Eng. Process. Process Intensif.*, **68** 38–44 (2013)
31. Schmitt, M, Baunach, M, Wengeler, L, Peters, K, Junges, P, Scharfer, P, Schabel, W, ''Slot-Die Processing of Lithium–Ion Battery Electrodes—Coating Window Characterization.'' *Chem. Eng. Process. Process Intensif.*, **68** 32–37 (2013)
32. Higgins, BG, Scriven, LE, ''Capillary Pressure and Viscous Pressure Drop Set Bounds on Coating Bead Operability.'' *Chem. Eng. Sci.*, **35** (3) 673–682 (1980)
33. Lee, SH, Koh, HJ, Ryu, BK, Kim, SJ, Jung, HW, Hyun, JC, ''Operability Coating Windows and Frequency Response in Slot Coating Flows from a Viscocapillary Model.'' *Chem. Eng. Sci.*, **66** (21) 4953–4959 (2011)
34. Durst, F, Wagner, H-G, ''Slot Coating.'' In: Kistler, SF, Schweizer, PM (eds.) *Liquid Film Coating*, pp. 401–426. Springer, Dordrecht (1997)
35. Cohen, ED, Gutoff, EB (eds.), *Modern Coating and Drying Technology*. VCH, New York, 1992